◆ Human Brain Mapping 19:224–247(2003) ◆

Three-Dimensional Maximum Probability Atlas of the Human Brain, With Particular Reference to the Temporal Lobe

Alexander Hammers,[1–3] Richard Allom,[1] Matthias J. Koepp,[1–3] Samantha L. Free,[2,3] Ralph Myers,[4] Louis Lemieux,[2] Tejal N. Mitchell,[2,3] David J. Brooks,[1] and John S. Duncan[2]*

[1]*MRC Clinical Sciences Centre and Division of Neuroscience, Faculty of Medicine, Imperial College, Hammersmith Hospital, London, United Kingdom*
[2]*Department of Clinical and Experimental Epilepsy, Institute of Neurology, UCL, Queen Square, London, United Kingdom*
[3]*National Society for Epilepsy MRI Unit, Chalfont St Peter, London, United Kingdom*
[4]*Imaging Research Solutions Ltd., Hammersmith Hospital, London, United Kingdom*

Abstract: Probabilistic atlases of neuroanatomy are more representative of population anatomy than single brain atlases. They allow anatomical labeling of the results of group studies in stereotaxic space, automated anatomical labeling of individual brain imaging datasets, and the statistical assessment of normal ranges for structure volumes and extents. No such manually constructed atlas is currently available for the frequently studied group of young adults. We studied 20 normal subjects (10 women, median age 31 years) with high-resolution magnetic resonance imaging (MRI) scanning. Images were nonuniformity corrected and reoriented along both the anterior-posterior commissure (AC–PC) line horizontally and the midsagittal plane sagittally. Building on our previous work, we have expanded and refined existing algorithms for the subdivision of MRI datasets into anatomical structures. The resulting algorithm is presented in the Appendix. Forty-nine structures were interactively defined as three-dimensional volumes-of-interest (VOIs). The resulting 20 individual atlases were spatially transformed (normalized) into standard stereotaxic space, using SPM99 software and the MNI/ICBM 152 template. We evaluated volume data for all structures both in native space and after spatial normalization, and used the normalized superimposed atlases to create a maximum probability map in stereotaxic space, which retains quantitative information regarding inter-subject variability. Its potential applications range from the automatic labeling of new scans to the detection of anatomical abnormalities in patients. Further data can be extracted from the atlas for the detailed analysis of individual structures. *Hum. Brain Mapping 19:224–247, 2003.* © 2003 Wiley-Liss, Inc.

Key words: brain mapping; methods; neuroanatomy; atlases; image processing, computer-assisted; anatomy, cross-sectional

A.H. and R.A. contributed equally to this work.

Contract grant sponsor: National Society for Epilepsy; Contract grant sponsor: Faculty of Medicine, Imperial College; Contract grant sponsor: Medical Research Council; Contract grant sponsor: Deutsche Forschungsgemeinschaft; Contract grant number: HA 3013/1-1.

*Correspondence to: Professor John S. Duncan, Department of Clinical and Experimental Epilepsy, Institute of Neurology, University College London, 33 Queen Square, London WC1N 3BG, UK. E-mail: j.duncan@ion.ucl.ac.uk

Received for publication 17 June 2002; Accepted 13 February 2003

DOI 10.1002/hbm.10123

INTRODUCTION

Functional imaging parameters need to be interpreted with reference to structural imaging data [Duncan and Fish, 1998]. For single subjects, correspondence between structure and function can be obtained through coregistration of functional imaging data with high-resolution structural imaging, typically magnetic resonance imaging (MRI). There are various coregistration methods available, all of which achieve sub-voxel accuracy [see Ashburner and Friston, 1997; Kiebel et al., 1997; Maes et al., 1997; Studholme et al., 1997; van den Elsen et al., 1993; Woods et al., 1993].

For group studies, this approach is only possible on a subject-by-subject basis, which generally requires time-consuming and observer-dependent region-of-interest analyses, or the use of regions defined by an atlas/template [Hammers et al., 2002]. For group studies using voxel-based analysis techniques, individual datasets are generally spatially transformed to a common frame of reference, a template in stereotaxic space, and statistical tests are applied to these spatially transformed images. Ascribing an anatomical localization to differences thus found between groups is difficult [Mazziotta et al., 1995], as any given single brain used for visualization may not be representative of the average anatomy.

Traditional neuroanatomy emphasized systems and their three-dimensional relationships [Lorente de Nó, 1934; Nieuwenhuys et al., 1988; Ramón y Cajal, 1929; Vesalius, 1543]. With the advent of positron emission tomography (PET), computed X-ray tomography (CT), and MRI, the emphasis has shifted to spatial relationships in the three orthogonal planes, which makes correct labeling of structures noticeably more difficult than when they are viewed three-dimensionally during dissection. Several printed atlases displaying two-dimensional neuroanatomy have been published to aid in correct labeling [for example, Duvernoy, 1991; Jackson and Duncan, 1996; Mai et al., 1997; Roberts and Hanaway, 1970; Schaltenbrand and Wahren, 1977; Talairach et al., 1967; Talairach and Tournoux, 1988]. Currently used template coordinates continue to be translated back, with debatable accuracy, into "Talairach coordinates" (online at http://www.mrc-cbu.cam.ac.uk/Imaging/mnispace.html) [Duncan et al., 2000]. This printed atlas, together with most others, and many earlier digital atlases [e.g., Adair et al., 1981; Bajcsy et al., 1983; Bohm et al., 1983; Dann et al., 1989; Evans et al., 1988, 1991; Gee et al., 1993; Greitz et al., 1991; Hammers et al., 2002; Miller et al., 1993; Rizzo et al., 1997; Sandor and Leahy, 1997; Seitz et al., 1990; Van Essen and Drury, 1997] share the disadvantage that they are derived from very few brains, typically one, or even, as in the case of the Talairach atlas, from a single hemisphere. Hemispheric asymmetries [Free et al., 2001; Geschwind and Galaburda, 1985; Good et al., 2001; Watkins et al., 2001] are not accounted for when only single hemispheres are used. A wide range of neuroanatomical variation, particularly in phylogenetically or ontogenetically younger structures, is well recognized in primates [Stephan et al., 1988] and will not be taken into account by atlases derived from few brains.

The recognition of these limitations has led to the development of templates derived from multiple, typically MRI, datasets [Evans et al., 1992, 1994] that are used principally for spatial transformation purposes. Due to averaging, they do not resolve cortical features well enough to enable exact anatomical labeling, despite sometimes being called atlases. Related labeled probabilistic maps based on larger numbers of subjects have been developed, but due to the amount of work involved in manual delineation, only automated extraction methods were used [Collins et al., 1999].

Recently, gyral pattern matching methods have been developed [Fischl et al., 1999; Thompson et al., 1997, 2001]. They resolve previously manually outlined gross cortical features well, even after averaging of many subjects. An atlas of cortical variability has thus been constructed from MRI data from 20 elderly controls [Thompson et al., 2001] in whom sulci are more easily resolved. This surface-based method does not, however, lend itself to volumetric studies of neuroanatomical structures or the investigation of subcortical structures. No corresponding variability data exists for younger healthy controls.

A further rationale for the development of a probabilistic or frequency-based, label-based atlas of neuroanatomy is to allow the statistical assessment of normal ranges for both structure volumes and spatial extents in native and stereotaxic space, to define a normal range against which patient groups may be compared.

The aims of this study were (1) to create a maximum probability map in stereotaxic space, and (2) to assess the descriptive volumetric statistics of the anatomical structures, both in native and in stereotaxic space.

SUBJECTS AND METHODS

Subjects

We studied 20 healthy volunteers from the database at the National Society for Epilepsy's MRI Unit. They had no neurological, medical, or psychiatric condition

and normal MRI studies as determined by two experienced neuroradiologists. There were 10 women (median age 30.5 years, mean ± SD 31.6 ± 9.9 years) and 10 men (median age 30.5 years, mean ± SD 31.5 ± 9.5 years). Ethical approval was obtained from the Joint Medical Ethics Committee of the Institute of Neurology and the National Hospital for Neurology and Neurosurgery, University College London, Queen Square, and all subjects had given written informed consent.

MRI acquisition

MRI scans were obtained on the 1.5 Tesla GE Signa Echospeed scanner at the National Society for Epilepsy. A coronal T1 weighted 3D volume was acquired using an inversion recovery prepared fast spoiled gradient recall sequence (GE), TE/TR/NEX 4.2 msec (fat and water in phase)/15.5 msec/1, time of inversion (TI) 450 msec, flip angle 20°, to obtain 124 slices of 1.5 mm thickness with a field of view of 18 × 24 cm with a 192 × 256 matrix. This covers the whole brain with voxel sizes of 0.9375 × 0.9375 × 1.5 mm. Nonuniformity correction was performed using a published method (N3) [Sled et al., 1998]. The images were then re-orientated with the horizontal line defined by the anterior and posterior commissures (AC–PC orientation) and the sagittal planes parallel to the midline as in previous studies [Moran et al., 1999; Sisodiya et al., 2001]. Images were resliced to create isotropic voxels of 0.9375 × 0.9375 × 0.9375 mm^3, using windowed sinc interpolation in order to preserve the native resolution. MRI datasets were segmented into gray matter, white matter, and CSF using a fully automatic algorithm (Exbrain) [Lemieux et al., 2003; Lemieux et al., 1999].

Creation of the refined and expanded (final) algorithm for anatomical subdivision

We have previously created a single brain atlas for which a delineation protocol for 39 structures had been developed and tested on five different datasets with voxel sizes of 2 × 2 × 2 mm^3 [Hammers et al., 2002]. This delineation algorithm has been expanded to include more structures. It has also been refined to take advantage of the smaller voxel sizes in this study, allowing for more precise anatomical delineation, and improving the definition of some structures. In the creation of the algorithm, we built on our previous work [Hammers et al., 2002; Niemann et al., 2000a] and standard atlases and textbooks of neuroanatomy [e.g., [Duvernoy, 1998, 1999; Jackson and Duncan, 1996; Kahle, 1986; Mai et al., 1997; Nieuwenhuys et al., 1988]. The list of all 49 structures and the delineation algorithm can be found in the Appendix.

Anatomical subdivision of the datasets

We used Sun Ultra 10 workstations (Sun Microsystems, Mountain View, CA) and Analyze AVW 3.1 [Robb and Hanson, 1991] for the creation of volumes of interest. The region-of-interest-module of the Analyze software allows definition of the borders of structures using a manually controlled cursor. We determined the optimum viewing intensity settings (level and width) for each MRI scan, chosen to be comparable among datasets, prior to any region definition, and noted them. They were subsequently applied every time a given MRI was analyzed. The CSF partition of the segmented MRIs was called up as a related volume to assist in the delineation of the ventricles. Oblique slices, i.e., parallel to the inferior surface of the temporal lobe, were used where appropriate to assist in the delineation of the sulci of the inferior temporal surface. All delineation was performed in native space, i.e., before spatial transformation into stereotaxic space. All 49 structures were delineated by one investigator (R.A.) on each MRI in turn before the next structure was commenced. After a given structure had been delineated on all 20 MRIs on both the left and right, the structures were reviewed to ensure that there had been no evolution in the interpretation of the protocol. In addition, a separate neuroanatomically trained operator (A.H.) evaluated each structure to ensure that consensus was reached in all difficult cases. Several general rules applied. For example, when a narrow sulcus was used as a boundary between adjacent structures, this common boundary was drawn along the midline of the sulcus to avoid systematic bias that would favor the apparent volume of the second structure delineated. Where sulci that were more than one voxel wide were used as common boundaries, however, each structure was individually defined up to the pia mater adjoining the sulcus. In delineating larger areas of neocortex, sulci that did not form boundaries were not followed into their depths, where they were generally less than one voxel wide.

Normalization of the individual atlases into stereotaxic space

The anatomical subdivision of the MRI datasets as described above yielded 20 separate atlases of neuroanatomy in native space, each containing 49 volumes of interest. Within each atlas, each voxel occurring

within a volume of interest has a numerical label between 1 and 49, whereas non-brain voxels have a label of zero. The corresponding MRI volumes were spatially normalized to a widely used T1 weighted MRI template in stereotaxic space, the Montreal Neurological Institute/International Consortium for Brain Mapping (MNI/ICBM) 152 standard, as contained in the Statistical Parametric Mapping (SPM99) package (Wellcome Department of Imaging Neuroscience, Institute of Neurology, UCL, London, UK, online at http://www.fil.ion.ucl.ac.uk/spm). This template preserves cerebral asymmetries [Evans et al., 1994]. Normalization was performed using the spatial processing routines contained within SPM99, implemented in Matlab version 5 (Mathworks Inc, Sherborn, MA) [Ashburner and Friston, 1997, 1999]. First, an affine linear transformation with 12 parameters (translation, rotation, scaling, and shear in each dimension) is performed. This is followed by nonlinear steps utilizing basis functions to accommodate inter-individual differences on a smaller scale. The widely used default settings [Ashburner and Friston, 1999; Meyer et al., 1999] of $7 \times 8 \times 7$ basis functions (representing x, y, and z dimensions in a three-dimensional coordinate system where x increases from left to right, y from posterior to anterior, and z from inferior to superior) and 12 iterations were chosen for our study. The spatial transformation module allows for the determination of the necessary warping steps from one image and their application to another one, which is in register. As the T1 weighted MRIs from which the individual atlases are derived are known, this can be exploited to transform the individual anatomical atlases. The normalized images were resampled with isotropic voxel sizes of $1 \times 1 \times 1$ mm^3 in a matrix of $x/y/z$ dimensions of 182/218/182 voxels. We used nearest neighbor interpolation to preserve unequivocal allocation of a given voxel to one VOI.

Preliminary statistical analysis

Structure volumes were extracted both in native and in stereotaxic space using Analyze AVW 3.1 [Robb and Hanson, 1991] The influence of sex on structure volumes was assessed using Student's t-tests, and the relationship between structure volumes, and age with Pearson's correlation coefficient. For comparison with previous studies, right–left differences were computed and their significance assessed using paired t-tests. Asymmetries of the frontal and occipital petalia were assessed by performing area measurements for the frontal lobe halfway between its most anterior extent and the most anterior slice containing the genu of the corpus callosum crossing the midline, and for the occipital lobe 10 slices (9.375 mm) anterior to its most posterior extent. As an example for stereotaxic coordinates for two structures in one direction of extension, we compared the maximum extents for the frontal lobe in anterior direction and occipital lobe in posterior direction. Descriptive statistics were calculated using Analyze AVW 3.1 and a standard statistical package (SPSS; SPSS, Chicago, IL). A P value of <0.05 was considered significant, without correction for multiple comparisons.

Creation of the maximum probability map in stereotaxic space

The probability of a particular voxel in stereotaxic space being occupied by a structure of interest can be ascertained by assessing the frequency of that structure residing at that voxel across the 20 datasets. Each structure delineated is identified by a unique assigned intensity, for example, the right hippocampus was assigned an intensity of one in all datasets, the left, two. Partial probabilities were avoided as we labeled the entire brain volume (see Fig. 1). We, therefore, computed the mode for each of the voxels of the normalized individual atlases, revealing the most frequently encountered object at each site and thereby creating a maximum probability map. Where two or more structures occurred with the same frequency at a given voxel, this voxel was randomly assigned one of the corresponding labels (see Discussion).

To obtain a visual impression of the improvement through inclusion of more datasets, four maximum probability maps were created, based on 5, 10, 15, and all 20 datasets, respectively.

RESULTS

The final delineation algorithm was successfully applied in all subjects without any alteration.

Structure volumes

The results (mean, SD), coefficient of variation (CV; defined as SD/mean) for all structures and the sum of all structures in native space as well as the corresponding values in stereotaxic space are shown in Table I. As expected, the variation of the total volume of all structures decreases markedly after spatial normalization (CV from 11 to 2%), whereas the effect of spatial normalization on the spread of the volumes of the structures is far less marked with an average CV of 18% in native space and 14% in stereotaxic space.

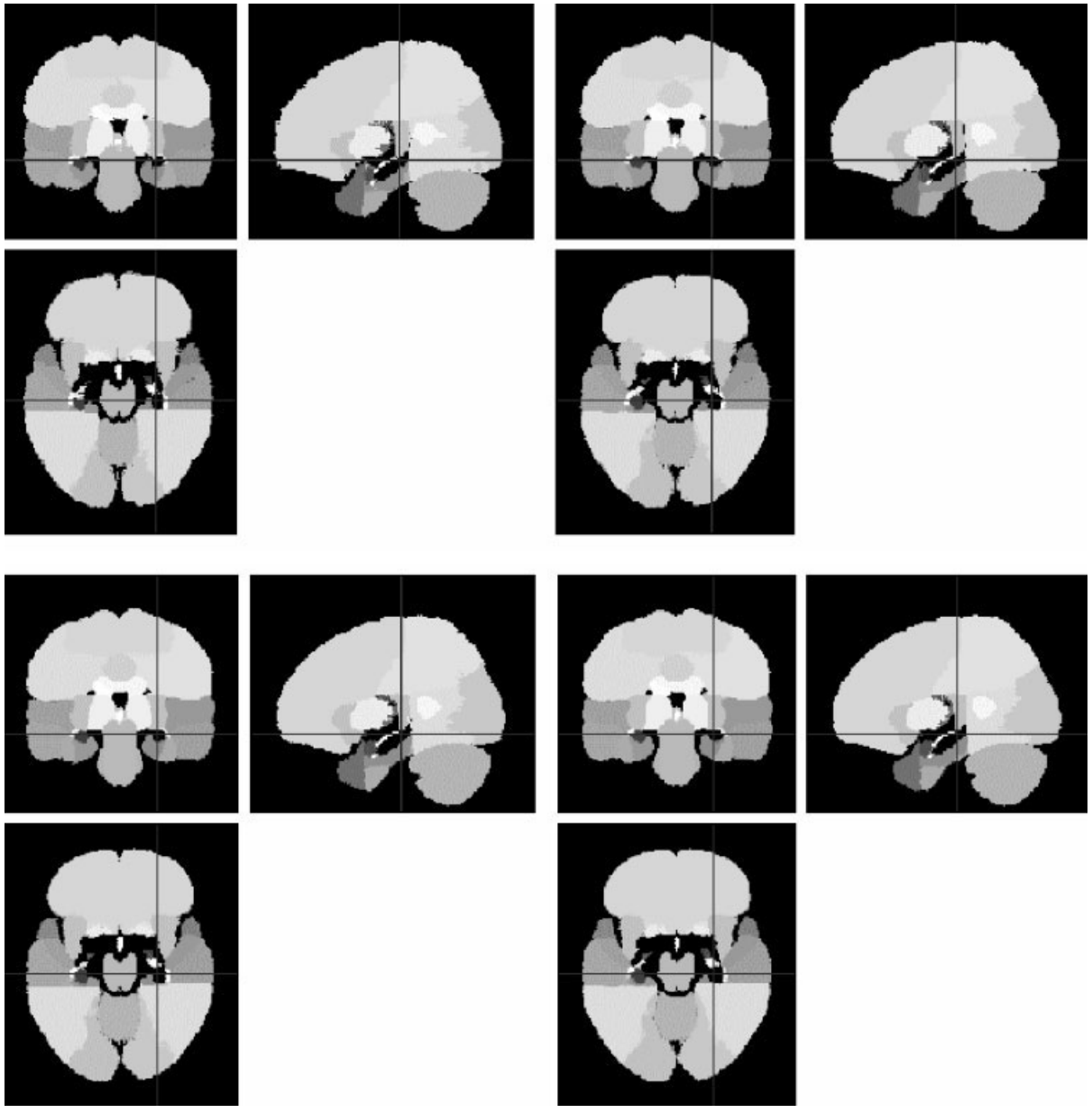

Figure 1.

Comparison of maximum probability maps obtained after inclusion of five subjects (**top left**), 10 subjects (**top right**), 15 subjects (**bottom left**), and all 20 subjects (**bottom right**). In general, while there is a marked improvement in border definition, indicated through the smoothness of the boundaries, from the five to ten subject version and a moderate further improvement through inclusion of 15 datasets, the difference between the 15 and 20 subject version is minimal. Some structures, e.g., the brainstem or the cerebellum, are very consistent across subjects and hardly change at all with inclusion of more subjects. Others are slightly more variable, e.g., the central sulcus or the occipital horn of the lateral ventricle, and there is appreciable improvement when more subjects are included. Finally, ill-defined boundaries, e.g., in the temporo-parieto-occipital area, do not become fully smooth even after inclusion of all 20 datasets. Crosshair indicates superoposterior right hippocampus.

Maximum probability maps in stereotaxic space

There were 37,900 occurrences of multiple modes while calculating the mode for all voxels, compared with a total of 1.9 million brain voxels contained within the normalized regions (2%).

The presentation of the atlas itself is necessarily in the form of a series of representative images. The four

TABLE I. Volumes of the different structures in native space and after normalization to a stereotaxic template.

		Original data			Spatially normalized data		
Area	Region	Mean (mm^3)	SD	CV	Mean (mm^3)	SD	CV
Temporal lobe	L amygdala	1638	300	0.18	2572	441	0.17
	R amygdala	1494	185	0.12	2347	328	0.14
	L ant lateral TL	8055	1369	0.17	11660	1567	0.13
	R ant lateral TL	8134	1597	0.20	11385	2149	0.19
	L ant medial TL	7148	1113	0.16	10579	1499	0.14
	R ant medial TL	7465	1343	0.18	10735	1912	0.18
	L fusiform gyrus	5165	1207	0.23	8412	1454	0.17
	R fusiform gyrus	4821	940	0.20	7967	1563	0.20
	L hippocampus	1996	297	0.15	3109	347	0.11
	R hippocampus	2251	364	0.16	3467	391	0.11
	L med + inf temp gyrus	17522	3106	0.18	27424	3312	0.12
	R med + inf temp gyrus	18726	3391	0.18	28989	3041	0.10
	L PH + ambient gyrus	4971	738	0.15	7711	766	0.10
	R PH + ambient gyrus	4775	761	0.16	7440	1019	0.14
	L posterior TL	59820	12959	0.22	85891	14055	0.16
	R posterior TL	60697	12559	0.21	88651	14472	0.16
	L superior temp gyrus	13078	2288	0.17	18909	2265	0.12
	R superior temp gyrus	13783	2178	0.16	19642	1912	0.10
Insula	L insula	14663	1857	0.13	20630	1193	0.06
	R insula	14574	2059	0.14	20296	1258	0.06
Frontal lobe	L ant cingulate gyrus	8426	1648	0.20	12731	3148	0.25
	R ant cingulate gyrus	8464	2008	0.24	12356	3055	0.25
	L frontal lobe	194371	24429	0.13	285793	6915	0.02
	R frontal lobe	195140	25355	0.13	289244	9222	0.03
Parietal lobe	L parietal lobe	126247	18613	0.15	183545	16148	0.09
	R parietal lobe	123500	17575	0.14	181217	11205	0.06
	L post cingulate gyrus	8155	1332	0.16	11416	1308	0.11
	R post cingulate gyrus	7927	1510	0.19	11293	2245	0.20
Occipital lobe	L occipital lobe	51710	8343	0.16	75443	11536	0.15
	R occipital lobe	53839	9911	0.18	77786	13122	0.17
Posterior fossa	L cerebellum	70259	6751	0.10	101327	4381	0.04
	R cerebellum	70860	7301	0.10	104407	4075	0.04
	Brainstem	24835	2906	0.12	34852	1806	0.05
Central structures	L accumbent nucleus	363	97	0.27	506	123	0.24
	R accumbent nucleus	326	100	0.31	479	124	0.26
	L caudate nucleus	4499	596	0.13	6571	957	0.15
	R caudate nucleus	4473	605	0.14	6606	1075	0.16
	L pallidum	1285	160	0.12	1784	205	0.11
	R pallidum	1431	304	0.21	1995	343	0.17
	L putamen	4421	567	0.13	6110	743	0.12
	R putamen	4456	546	0.12	6295	635	0.10
	L thalamus	7784	870	0.11	11167	882	0.08
	R thalamus	7420	812	0.11	10517	1109	0.11
	Corpus callosum	21646	2983	0.14	30887	3907	0.13
Ventricles	Body of L lat ventricle	7893	2411	0.31	11303	2333	0.21
	Body of R lat ventricle	7206	2880	0.40	10133	2376	0.23
	L temporal horn	559	150	0.27	896	198	0.22
	R temporal horn	643	128	0.20	1018	166	0.16
	Third ventricle	1034	306	0.30	1462	366	0.25
	Total regional volume	1289861	147973	0.11	1886954	37986	0.02

SD, standard deviation; R, right; L, left; CV, coefficient of variation (SD/Mean); ant, anterior; post, posterior; sup, superior; inf, inferior; med, medial; lat, lateral; TL, temporal lobe; PH, parahippocampal.

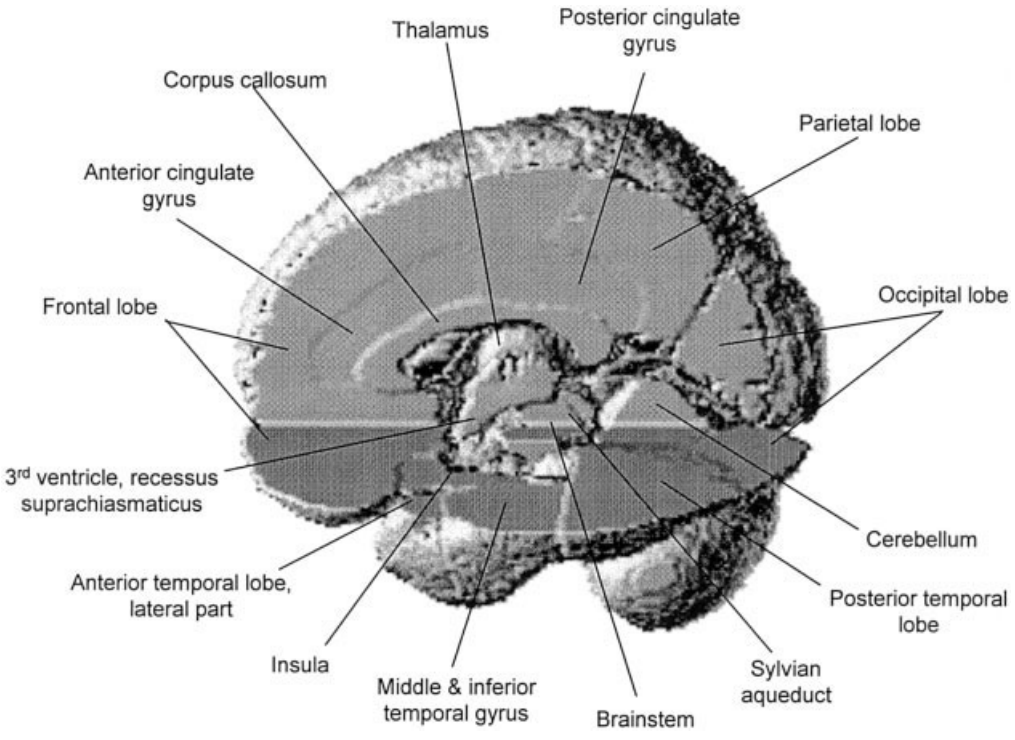

Figure 2.
Labeled three-dimensional rendering of the maximum probability atlas revealing some of the internal detail.

maximum probability maps constructed using 5, 10, 15, and all 20 datasets, respectively, are shown in Figure 1. The smoothness of the boundaries, indicating the precision of the boundary estimate, increases markedly from the first map (five datasets) to the second map (10 datasets) and moderately from the second to the third map (15 datasets), while the improvement from the third to the final map (20 datasets) is subtle. Figure 1 also shows that easily defined, relatively constant features of human neuroanatomy such as the contours of the brain or the central sulcus appear smooth after inclusion of relatively few datasets, whereas boundaries of structures that are more difficult to define such as the lateral occipital-parietal border only become smooth after inclusion of all 20 datasets. Figure 2 shows a three-dimensional rendering of the maximum probability atlas revealing some of the internal detail, for example, the sylvian aqueduct or the suprachiasmatic recessus of the third ventricle.

Examples of more detailed analysis

The measured brain structures were an average of 16% larger in men. This difference was significant in 28/44 gray/white matter regions and 4/5 ventricular regions. There was no significant correlation with age in any of the 49 regions. Significant right–left differences were found in 7/23 paired structures (excluding the unpaired structures brainstem, corpus callosum and third ventricle). The following structures were bigger than their contralateral counterparts: right hippocampus (13%), left amygdala (9%), right superior temporal gyrus (5%), right middle and inferior temporal gyrus (7%), left thalamus (5%), left pallidum (11%), and right temporal horn (15%).

Investigation of the petalia as described in Materials and Methods showed significant side-to-side differences. Right sided frontal petalia were an average of 4% bigger than their left counterparts, and 13/20 subjects showed this side difference, while the left occipital petalia was bigger than the right by an average of 16%, and this side difference was present in 15/20 subjects.

There were no average differences in the maximum anterior extent of the right and left frontal lobes. The left occipital lobe extended an average of 0.7 mm further posterior than the right; this difference was not significant.

DISCUSSION

We present the first fully manually constructed, label-based maximum probability atlas of the human

brain, designed for the younger adult age group that is frequently studied in functional neuroimaging studies.

Algorithm and anatomical subdivision

The major drawback of any manual labeling method is the strain it puts on human resources. At the resolution used in this study, it took one operator around 30 h to segment a single MRI dataset. We, therefore, restricted ourselves to the 49 structures presented here. This report introduces the concept of the construction of a maximum probability map and focuses on the temporal lobe, reflecting our interest in epilepsy. The current lack of further lobar subdivisions of the frontal, parietal, and occipital lobes is a limitation, particularly where anatomical subdivisions correlate with functional specialization. Work to extend the concept presented here to the other principle lobes can build on more detailed anatomical subdivisions presented in earlier reports by other groups [e.g., Chiavaras et al., 2001; Crespo-Facorro et al., 2000; Kennedy et al., 1998; Tomaioulo et al., 1999].

The current version of the atlas combines gray and associated white matter for most cortical areas. Automated software to segment T1 weighted MRI images is readily available [e.g,. Ashburner and Friston, 1997; Lemieux, 2001; Lemieux et al., 1999], and this information can be used to create pure gray matter, white matter, or CSF versions of the atlas if required.

Non-automatic methods are subject to bias. There is currently no other way, however, to reliably incorporate expert knowledge into the definition of anatomical structures. We have tried to limit subjectivity as far as possible: To avoid bias through different orientations of raw data, in addition to careful acquisition, we used rigid body reorientation prior to delineation. We created a detailed, written protocol to which we consistently adhered. Publication of protocols is essential [Bergin et al., 1994] as it allows the comparison of other investigators' results; differences in boundary definition can be assessed and quantified. To avoid bias through different intensity settings, the optimum viewing intensity was applied every time a given MRI was analyzed. We measured each structure in turn and reviewed it after completion of all 20 datasets, to ensure there had been no evolution in the interpretation of the protocol. Difficult structures to define were noted and a consensus reached between the two main investigators (R.A., A.H.). Segmented images and oblique slices were used where appropriate to ensure optimum reproducibility.

We have not performed formal intra-rater and inter-rater reliability studies. We were, however, able to compare the volumetric results obtained for hippocampus, amygdale, and temporal horn with results obtained with the same protocol in a previous study [Niemann et al., 2000a]. The volumes for these structures obtained in the current study corresponded well, with the hippocampi being an average of 5.9% and the amygdalae an average of 4.4% larger. This volume increase (and corresponding 15% volume decrease of the temporal horns) reflects the smaller voxel size used in the current study, which minimizes partial volume effects and permits better delineation of the margins of a volume. Accordingly, the right–left asymmetry of the hippocampus and the temporal horns were replicated.

Normalization of individual atlases into stereotaxic space

Both the choice of the stereotaxic frame of reference and the choice of software and settings used for the spatial transformations have a direct influence on the results obtained. The MNI152 template was chosen as it is deemed to be representative of normal anatomy through the use of 152 MRI datasets in its construction and preserves asymmetry [Evans et al., 1994]. The MNI templates are known to be larger than the Talairach hemisphere (online at http://www.mrc-cbu.cam.ac.uk/Imaging/mnispace.html) [Ashburner et al., 1997]. Our data quantifies this difference for 20 healthy controls. The total regional volume was 46% bigger, which, assuming equal differences in each direction, corresponds to an average 13.5% increase in each dimension (Table I). For comparison, another group found the linear zooms for affine transformations of 51 normal brains to a single subject MRI dataset brought into MNI/ICBM space to be 1.10 in mediolateral direction, 1.05 in anteroposterior direction, and 1.17 in dorsoventral direction [Ashburner et al., 1997].

For the spatial transformations, we chose SPM99, using the widely used default settings and optimizing the process by manually defining the anterior commissure as the starting point for estimation. SPM99 and the current version of the maximum probability atlas can be used in combination. As regions were defined in native space, any future combination of template (e.g., more representative of normal brain size) and spatial transformation software can be used to create further versions.

The MNI templates are available for T1 weighted, T2 weighted and proton density images. If the maxi-

mum probability map was to be used for other data brought into MNI space (e.g., EPI for which there is a template delivered with SPM99), its accuracy would be influenced by the way such a template was created and ultimately by the degree to which such a template is truly in register with the MNI templates.

Characteristics of the regional data obtained

The different structures had different variabilities (Table I). This regional variation has various sources: Firstly, some structures, for example brainstem and cerebellum, are likely to be intrinsically less variable than brain areas that mature later, for example, association cortices. Secondly, some structures have more clearly defined boundaries than others. For example, the central sulcus and the outer surface of the brain can be determined with great precision, whereas there is no clear boundary between posterior temporal lobe and occipital/parietal cortex. Thirdly, larger regions tend to have smaller surface-to-volume ratios, allowing less variability through delineation of the surface boundaries.

A limitation of the current study is that the various sources for regional variation cannot be precisely distinguished. Such studies have been performed in several anatomical areas (see Comparison With Previous Work) but the attempt to investigate this for the whole brain was beyond the scope of this study.

The normalization process corrects mainly the variation in total brain volume but maintains regional variability (Table I), indicating the usefulness of assessing volumetric differences between groups of subjects in stereotaxic space.

Our preliminary statistical analysis was aimed at establishing comparability of our results with previously published studies. As expected, we found the well-established volume differences between brains from male and female subjects [for a review, see Good et al., 2001]; no influence of age for this homogenous sample of younger adults; and we replicated known right–left differences for structure volumes [e.g. Niemann et al., 2000a; for a review, see Good et al., 2001] as well as for the frontal and occipital petalia. The finding of positional differences for the maximum posterior extent of the occipital lobe but not the maximum anterior extent of the frontal lobe is in good agreement with the data from the ICBM/MNI templates used within SPM99. It also shows one of the potential applications of the data collected in this study, i.e., investigation of stereotaxic coordinates. Providing full probabilistic information for all structures in all planes, however, is well beyond the scope of a journal contribution. It may be extracted from the electronic version of the data.

Creation of the maximum probability map in stereotaxic space

In the computation of the mode for each voxel, we used the convention that if two or more values occurred with the same frequency, one of the values would be chosen randomly. Most structures have a small surface/volume ratio, and this convention was only used in those 2% of voxels for which no unequivocal mode existed. Most of these lie on the outer surface of the brain. We initially used a cruder approach of always assigning the biggest of two or more modes. This initial approach can be seen as maximally biased. The mean difference between structure volumes obtained using both assignment algorithms was 0.09%, i.e., had we used the initial maximally biased approach, the anatomical structures' volume would only have increased by an average factor of 1.0009, which is negligible compared to biological variation.

Even with the limited number of subjects included, considerable detail emerges in the maximum probability map, indicating good inter-subject positional correspondence following the spatial normalization procedure. Many features, for example, the course of the aqueduct as a landmark in the midbrain (Fig. 2), or the position of the middle genu of the central sulcus and the hand knob of the precentral gyrus [Yousry et al., 1997], will be useful in functional neuroimaging.

Comparison with previous work

Collins et al. [1999] have described a probabilistic atlas based on a larger number of subjects. While they acknowledged that, ideally, manual segmentations of all atlas structures on all subjects should be used, due to time constraints, these workers used an automatic procedure to segment their datasets into anatomical regions. It would be interesting to compare the maximum probability maps obtained with the two methods to see whether the automatic method yields comparable results in terms of volumes and spatial coordinates. The extension of our work to very large numbers of subjects is hardly feasible, whereas their automatic approach would lend itself to such an extension.

A widely used work of reference has investigated the frequency of occurrence of different sulcal patterns [Ono et al., 1990] based on 25 postmortem brains. While being useful, this suffers the disadvantages of printed atlases, e.g., difficulty of access and limitation

of data shown, and does not investigate the volumes of structures defined by the sulcal boundaries investigated. A variety of studies of small brain regions have been published that investigate volumes, surfaces, sulcal patterns, or subcortical structures in more detail [e.g., Amunts et al., 2000; Andrew and Watkins, 1969; Brierley and Beck, 1959; Chiavaras et al., 2001; Filimonoff, 1932; Geyer et al., 1999, 2000; Grefkes et al., 2001; Kim et al., 2000; Lohmann et al., 1999; Morosan et al., 2001; Niemann et al., 2000b; Niemann and van Nieuwenhofen, 1999; Paus et al., 1996; Penhune et al., 1996; Rademacher et al., 2001a; Rademacher et al., 1993; Rademacher et al., 2001b; Steinmetz et al., 1990; Thompson et al., 1996; Tomaioulo et al., 1999; Van Buren and Maccubbin, 1962; Westbury et al., 1999; Zilles et al., 1997]. Such approaches have been shown to be useful for the probabilistic localization of anatomical or functional areas of the brain [e.g., Fox et al., 2001; Paus et al., 1996; Van Essen et al., 2001]. Some further studies have investigated volumes of neuroanatomical structures without assessing variability in a stereotaxic reference coordinate system [e.g., Crespo-Facorro et al., 2000; Kennedy et al., 1998; Lange et al., 1997], while others have defined neuroanatomical structures in various stereotaxic spaces without incorporating probabilistic information [e.g., Hammers et al., 2002; Talairach and Tournoux, 1988; Tzourio-Mazoyer et al., 2002].

The development of an atlas incorporating macroscopic in vivo and microscopic in vitro data as well as blood flow activation imaging and other functional information, demographic and genetic information derived from a very large number of subjects by largely automated methods has been pursued since the early 1990s by the International Consortium for Brain Mapping [Mazziotta et al., 1995, 2001]. This data collection will be a very useful tool when it becomes available. The work presented here, incorporating manual segmentations of the entire brain, should be regarded as complementary.

A different type of information is being extracted in projects looking at cortical variability using gyral pattern matching [Thompson et al., 1997, 2001]. This approach achieves exact correspondence of a limited number of previously manually extracted sulci for subsequent measurements of parameters like amount of gray matter at a location defined through its relative distance from the mapped landmarks. In contrast to the approach used here, Thompson et al. achieve "exact" mapping of the sulcal landmarks, with ensuing "crisp" appearance of cortical features even after averaging of many subjects. The approach assumes a one-to-one correspondence, however, and their approach, although generalizable in principle, has so far only been applied to the cortical surface and the hippocampus, with no subcortical or volumetric studies. Again, the approaches should be considered complementary.

Further to the use of the maximum probability map to automatically segment structural and functional brain imaging data sets into anatomical regions [Hammers et al., 2002], there are several other potential applications.

First, as the maximum probability map is fully three-dimensional and in register with the ICBM/MNI templates used within SPM99, it can be used to overlay results of group studies [Tzourio-Mazoyer et al., 2002], giving probability-based information based on a sample of 20 healthy controls. This is a significant methodological advance compared to the translation of the coordinates obtained into a stereotaxic coordinate system based on one hemisphere [Talairach and Tournoux, 1988]. The accuracy will partly depend on the type of original data used and may be lower for data with low spatial resolution (e.g., SPECT) or distortions (e.g., EPI). Use of automatical labeling will be greatest in areas where the anatomical boundaries necessarily used in the creation of this atlas correspond best to functional boundaries.

Secondly, the stereotaxically normalized versions of the individual atlases contain the full probabilistic information for any given voxel. This can be exploited for region-based partial volume correction methods [e.g., Labbé et al., 1998; Rousset et al., 1995] in which calculation of absolute parameters of functional imaging data can be based not only on an individual voxel's tissue class probability but also its population-based probabilistic anatomical classification.

A third potential application is the use of the probabilistic information obtained here for the detailed analysis of individual structures. By creating "probability shells" corresponding to certain percentile probabilities or by obtaining measures of linear extent or spatial relationship to reference landmarks such as the anterior and posterior commissure, information can be obtained on the range of normal anatomy. This information can then be further used for the comparison of patients in whom an alteration of shape or volume of a particular brain structure or region is suspected.

ACKNOWLEDGMENTS

This work was supported in part by the Faculty of Medicine, Imperial College (BSc Clinical Sciences Program). We are grateful to our colleagues in the Cyclotron Building (especially Richard Banati, John Aston,

Kris Thielemans, and Federico Turkheimer) for help in the creation of the atlas, our colleagues at the National Society for Epilepsy for acquisition and preparation of the MRI datasets, Drs. Brian Kendall and John Stevens for neuroradiological evaluation of the MRIs, and all our volunteers for their participation.

REFERENCES

Adair T, Karp P, Stein A, Bajcsy R, Reivich M. (1981):Technical note. Computer assisted analysis of tomographic images of the brain. J Comput Assist Tomogr 5:929–932.

Amunts K, Malikovic A, Mohlberg H, Schormann T, Zilles K. (2000): Brodmann's areas 17 and 18 brought into stereotaxic space: where and how variable? Neuroimage 11:66–84.

Andrew J, Watkins ES. (1969): A stereotaxic atlas of the human thalamus and adjacent structures. A variability study. Baltimore: Williams & Wilkins.

Ashburner J, Friston KJ. (1997): Multimodal image coregistration and partitioning: a unified framework. Neuroimage 6:209–217.

Ashburner J, Friston KJ. (1999): Nonlinear spatial normalization using basis functions. Hum Brain Mapp 7:254–266.

Ashburner J, Neelin P, Collins DL, Evans A, Friston K. (1997): Incorporating prior knowledge into image registration. Neuroimage 6:344–352.

Bajcsy R, Lieberson R, Reivich M. (1983): A computerized system for the elastic matching of deformed radiographic images to idealised atlas images. J Comput Assist Tomogr 7:618–625.

Bergin PS, Raymond AA, Free SL, Sisodiya SM, Stevens JM. (1994): Magnetic resonance volumetry. Neurology 44:1770–1771.

Bohm C, Greitz T, Kingsley D, Berggren BM, Olsson L. (1983): Adjustable computerized stereotaxic brain atlas for transmission and emission tomography. AJNR Am J Neuroradiol 4:731–733.

Brierley JB, Beck E. (1959): The significance in human stereotactic brain surgery of individual variation in the diencephalon and globus pallidus. J Neurol Neurosurg Psychiatr 22:287–298.

Chiavaras MM, LeGoualher G, Evans A, Petrides M. (2001): Three-dimensional probabilistic atlas of the human orbitofrontal sulci in standardized stereotaxic space. Neuroimage 13:479–496.

Collins DL, Zijdenbos AP, Baaré WFC, Evans AC. (1999): ANIMAL+INSECT: Improved cortical structure segmentation. LNCS 1613:210–223.

Crespo-Facorro B, Kim J-J, Andreasen NC, Spinks R, O'Leary D, Bockolt HJ, et al. (2000): Cerebral cortex: a topographic segmentation method using magnetic resonance imaging. Psychiatry Res 100:97–126.

Dann R, Hoford J, Kovacic S, Reivich M, Bajcsy R. (1989): Evaluation of elastic matching system for anatomic (CT, MR) and functional (PET) cerebral images. J Comput Assist Tomogr 13:603–611.

Duncan J, Seitz RJ, Kolodny J, Bor D, Herzog H, Ahmed A, et al. (2000): A neural basis for general intelligence. Science 289:457–460.

Duncan JS, Fish DR. (1998): Integration of structural and functional data. Curr Opin Neurol 11:119–122.

Duvernoy HM. (1991): The human brain. Surface, three-dimensional sectional anatomy, and MRI. New York: Springer Verlag.

Duvernoy HM. (1998): The human hippocampus. Functional anatomy, vascularization and serial sections with MRI. NewYork: Springer.

Duvernoy HM.(1999): The human brain. Surface, blood supply, and three-dimensional sectional anatomy. New York: Springer.

Evans AC, Beil C, Marrett S, Thompson CJ, Hakim A. (1988): Anatomical-functional correlation using an adjustable MRI-based region of interest atlas with positron emission tomography. J Cereb Blood Flow Metab 8:513–530.

Evans AC, Collins DL, Milner B. (1992): An MRI-based stereotactic brain atlas from 300 young normal subjects. Proc 22nd Annu Symp Soc Neurosci 1992:408.

Evans AC, Kamber M, Collins DL, MacDonald D. (1994): An MRI-based probabilistic atlas of neuroanatomy. In: Shorvon SD, Fish DR, Andermann F, Bydder GM, Stefan H, editors. Magnetic resonance scanning and epilepsy. New York: Plenum Press. p 263–274.

Evans AC, Marett S, Torrescorzo J, Ku S, Collins L. (1991): MRI-PET correlation in three dimensions using a volume-of-interest (VOI) atlas. J Cereb Blood Flow Metab 11:A69–A78.

Filimonoff IN. (1932): Über die Variabilität der Grosshirnrindenstruktur. Mitteilung II. Regio occipitalis beim erwachsenen Menschen. J Psychol Neurol 44:1–96.

Fischl B, Sereno MI, Tootell RBH, Dale AM. (1999): High-resolution inter-subject averaging and a coordinate system for the cortical surface. Hum Brain Mapp 8:272–284.

Fox PT, Huang A, Parsons LM, Xiong JH, Zamarippa F, Rainey L, et al. (2001): Location-probability profiles for the mouth region of human primary motor-sensory cortex: model and validation. Neuroimage 13:196–209.

Free SL, O'Higgins P, Maudgil DD, Dryden IL, Lemieux L, Fish DR, et al. (2001): Landmark-based morphometrics of the normal adult brain using MRI. Neuroimage 13:801–813.

Gee JC, Reivich M, Bajcsy R. (1993): Elastically deforming 3D atlas to match anatomical brain images. J Comput Assist Tomogr 17: 225–236.

Geschwind N, Galaburda AM. (1985): Cerebral lateralization. Biological mechanisms, associations, and pathology: I. A hypothesis and a program for research. Arch Neurol 42:428–459.

Geyer S, Schleicher A, Zilles K. (1999): Areas 3a, 3b, and 1 of human primary somatosensory cortex. 1. Microstructural organization and interindividual variability. Neuroimage 10:63–83.

Geyer S, Schormann T, Mohlberg H, Zilles K. (2000): Areas 3a, 3b, and 1 of human primary somatosensory cortex. 2. Spatial normalization to standard anatomical space. Neuroimage 11:684–696.

Good CD, Johnsrude I, Ashburner J, Henson RNA, Friston KJ, Frackowiack RSJ. (2001): Cerebral asymmetry and the effects of sex and handedness on brain structure: a voxel-based morphometric analysis of 465 normal adult human brains. Neuroimage 14:685–700.

Grefkes C, Geyer S, Schormann T, Roland P, Zilles K. (2001): Human somatosensory area 2: ovserver-independent cytoarchitectonic mapping, interindividual variability, and population map. Neuroimage 14:617–631.

Greitz T, Bohm C, Holte S, Eriksson L. (1991): A computerized brain atlas: Construction, anatomical content, and some applications. J Comput Assist Tomogr 15:26–38.

Hammers A, Koepp MJ, Free SL, Brett M, Richardson MP, Labbé C, et al. (2002): Implementation and application of a brain template for multiple volumes of interest. Hum Brain Mapp 15:165–174.

Jackson GD, Duncan JS. (1996): MRI neuroanatomy: A new angle on the brain. London: Churchill Livingstone.

Kahle W. (1986): Nervensysteme und Sinnesorgane, Vol 3. New York: Georg Thieme Verlag.

Kennedy DN, Lnage N, Makris N, Bates J, Meyer J, Caviness VSJ. (1998): Gyri of the human neocortex: an MRI-based analysis of volume and variance. Cereb Cortex 8:372–384.

Kiebel SJ, Ashburner J, Poline JB, Friston KJ. (1997): MRI and PET coregistration: a cross validation of statistical parametric mapping and automated image registration. Neuroimage 5:271–279.

Kim JJ, Crespo-Facorro B, Andreasen NC, O'Leary DS, Zhang B, Harris G, et al. (2000): An MRI-based parcellation method for the temporal lobe. Neuroimage 11:271–288.

Labbé C, Koepp MJ, Ashburner J, Spinks TJ, Richardson MP, Duncan JS, et al. Absolute PET quantification with correction for partial volume effects within cerebral structures. In: Carson C, Daube-Witherspoon M, Herscovitch P, editors. Quantitative functional brain imaging with positron emission tomography. San Diego: Academic Press. p 59–66.

Lange N, Gjedd JN, Castellanos FX, Vaituzis AC, Rapoport JL. (1997): Variability of human brain structure size: ages 4–20 years. Psychiatry Res 74:1–12.

Lemieux L, Hammers A, MacKinnon T, Liu RS. (2003): Automatic segmentation of the brain and intracranial cerebrospinal fluid in T1-weighted volume MRI scans of the head, and its application to serial cerebral and intracranial volumetry. Magn Reson Med 49: 872–884.

Lemieux L, Hagemann G, Krakow K, Woermann FG. (1999): Fast, accurate, and reproducible automatic segmentation of the brain in T_1-weighted volume MRI data. Magn Reson Med 42:127–135.

Lohmann G, Yves von Cramon D, Steinmetz H. (1999): Sulcal variability of twins. Cerebral Cortex 9:754–763.

Lorente de Nó R. (1934): Studies on the structure of the cerebral cortex. II: Continuation of the study of the Ammonic system. J Psychol Neurol 46:113–177.

Maes F, Collignon A, Vandermeulen D, Marchal G, Suetens P. (1997): Multimodality image registration by maximazation of mutual information. IEEE Trans Med Imag 16:187–198.

Mai JK, Assheuer J, Paxinos G. (1997): Atlas of the human brain. Boston: Academic Press.

Mazziotta JC, Toga AW, Evans AC, Fox P, Lancaster J. (1995): A probabilistic atlas of the human brain: Theory and rationale for its development. Neuroimage 2:89–101.

Mazziotta J, Toga A, Evans A, Fox P, Lancaster J, Zilles K, et al. (2001): A probabilistic atlas and reference system for the human brain: International Consortium for Brain Mapping (ICBM). Phil Trans R Soc Lond B Biol Sci 356:1293–1322.

Meyer JH, Gunn RN, Myers R, Grasby PM. (1999): Assessment of spatial normalization of PET ligand images using ligand-specific templates. Neuroimage 9:545–553.

Miller MI, Christensen GE, Amit Y, Grenander U. (1993): Mathematical textbook of deformable neuroanatomies. Proc Natl Acad Sci U S A 90:11944–11948.

Moran NF, Lemieux L, Maudgil D, Kitchen ND, Fish DR, Shorvon SD. (1999): Analysis of temporal lobe resections in MR images. Epilepsia 40:1077–1084.

Morosan P, Rademacher J, Schleicher A, Amunts K, Schormann T, Zilles K. (2001): Human primary auditory cortex: cytoarchitectonic subdivisions and mapping into a spatial reference system. Neuroimage 13:684–701.

Niemann K, van Nieuwenhofen I. (1999): One atlas, three anatomies: relationships of the Schaltenbrand and Wahren microscopic data. Acta Neurochir (Wien) 141:1025–1038.

Niemann K, Hammers A, Coenen VA, Thron A, Klosterkötter J. (2000a): Evidence for smaller left hippocampus and left temporal horn in both patients with first episode schizophrenia and normal controls. Psychiatry Res Neuroimaging 99:93–110.

Niemann K, Mennicken VR, Jeanmonod D, Morel A. (2000b): The Morel stereotactic atlas of the human thalamus: Atlas-to-MR registration of internally consistent canonical model. Neuroimage 12:601–616.

Nieuwenhuys R, Voogd J, van Huijzen C. (1988): The human central nervous system. A synopsis and atlas. NewYork: Springer-Verlag.

Ono M, Kubik S, Abernathey CD. (1990): Atlas of the cerebral sulci. New York: Georg Thieme Verlag.

Paus T, Otaky N, Caramanos Z, MacDonald D, Zijdenbos A, D'Avirro D, et al. (1996): In vivo morphometry of the intrasulcal gray matter in the human cingulate, paracingulate and superior rostral sulci: hemispheric asymmetries, gender differences and probability maps. J Comp Neurol 376:664–673.

Penhune VB, Zatorre RJ, MacDonald JD, Evans AC. (1996): Interhemispheric anatomical differences in human primary auditory cortex: Probabilistic mapping and volume measurement from MR scans. Cerebral Cortex 6:617–672.

Rademacher J, Caviness VS, Steinmetz H, Galaburda AM. (1993): Topographical variation of the human primary cortices: implications for neuroimaging, brain mapping and neurobiology. Cerebral Cortex 3:313–329.

Rademacher J, Burgerl U, Geyer S, Schormann T, Schleicher A, Freund HJ, et al. (2001a): Variability and asymmetry in the human precentral motor system: a cytoarchitectonic and myeloarchitectonic brain mapping study. Brain 124:2232–2258.

Rademacher J, Morosan P, Schormann T, Schleicher A, Werner C, Freund HJ, et al. (2001b): Probabilistic mapping and volume measurement of human primary auditory cortex. Neuroimage 13:669–683.

Ramón y Cajal S. (1929): Etudes sur la neurogenèse de quelques vertébrés: recueil de mes principales recherches concernant la genèse des nerfs, la morphologie et la structure neuronale, l'origine de la névroglie, les terminaisons nerveuses sensorielles, etc. Madrid: Tipografía Artística.

Rizzo G, Scifo P, Gilardi MC, Bettinardi V, Grassi F, Cerutti S, et al. (1997): Matching a computerized brain atlas to multimodal medical images. Neuroimage 6:59–69.

Robb RA, Hanson DP. (1991): A software system for interactive and quantitative visualization of multidimensional biomedical images. Australas Phys Eng Sci Med 14:9–30.

Roberts M, Hanaway J. (1970): Atlas of the human brain in section. Philadelphia: Lea and Feibiger.

Rousset OG, Ma Y, Marenco S, Wong DF, Evans AC. (1995): In vivo correction for partial volume effects in PET: accuracy and precision. Neuroimage 2:S33.

Sandor S, Leahy R. (1997): Surface-based labeling of cortical anatomy using a deformable atlas. IEEE Trans Med Imaging 16:41–54.

Schaltenbrand G, Wahren W. (1977): Atlas for stereotaxy of the human brain. Chicago: Year Book Medical Publishers.

Seitz RJ, Bohm C, Greitz T, Roland PE, Eriksson L, Blomqvist G, et al. (1990): Accuracy and precision of the computerized brain atlas programme for localization and quantification in positron emission tomography. J Cereb Blood Flow Metab 10:443–457.

Sisodiya SM, Free SL, Williamson KA, Mitchell TN, Willis C, Stevens JM, et al. (2001): PAX6 haploinsufficiency causes cerebral malformation and olfactory dysfunction in humans. Nat Genet 28:214–216.

Sled JG, Zijdenbos AP, Evans AC. (1998): A nonparametric method for automatic correction of intensity nonuniformity in MRI data. IEEE Trans Med Imag 17:87–97.

Steinmetz H, Furst G, Freund HJ. (1990): Variation of perisylvian and calcarine anatomic landmarks within stereotactic proportional coordinates. AJNR Am J Neuroradiol 11:1123–1130.

Stephan H, Baron G, Frahm HD. (1988): Comparative size of brains and brain components. In: Steklis HD, Erwin J, editors. Neurosciences, Vol 4. New York: Alan R. Liss, Inc. p 1–38.

Studholme C, Hill DLG, Hawkes DJ. (1997): Automated three-dimensional registration of magnetic resonance and positron emission tomography brain images by multiresolution optimization of voxel similarity measures. Med Phys 24:25–35.

Talairach J, Tournoux P. (1988): Co-planar stereotaxic atlas of the human brain. New York: Georg Thieme Verlag.

Talairach J, Szikla G, Tournoux P, Prossalentis A, Bornas-Ferrier M. (1967): Atlas d'anatomie stéréotaxique du télencéphale. Etudes anatomo-radiologiques. Paris: Masson.

Thompson PM, Schwartz C, Lin RT, Khan AA, Toga AW. (1996): Three-dimensional statistical analysis of sulcal variability in the human brain. J Neurosci 16:4261–4274.

Thompson PM, MacDonald D, Mega MS, Holmes CJ, Evans AC, Toga AW. (1997): Detection and mapping of abnormal brain structure with a probabilistic atlas of cortical surfaces. J Comput Assist Tomogr 4:567–581.

Thompson PM, Mega MS, Woods RP, Zoumalan CI, Lindshield CJ, Blanton RE, et al. (2001): Cortical change in Alzheimer's disease detected with a disease-specific population-based brain atlas. Cereb Cortex 11:1–16.

Tomaioulo F, MacDonald JD, Caramanos Z, Posner G, Chiavaras M, Evans AC, et al. (1999): Morphology, morphometry and probability mapping of the pars opercularis of the inferior frontal gyrus: an in vivo MRI analysis. Eur J Neurosci 11:3033–3046.

Tzourio-Mazoyer N, Landeau B, Papathanassiou D, Crivello F, Etard O, Delcroix N, et al. (2002): Automated anatomical labeling of activations in SPM using a macroscopic anatomical parcellation of the MNI MRI single-subject brain. Neuroimage 15:273–289.

Van Buren J, Maccubbin D. (1962): An outline atlas of the human basal ganglia with estimation of anatomical variants. J Neurosurg 19:811–839.

van den Elsen PA, Pol E-JD, Viergever MA. (1993): Medical image matching: a review with classification. IEEE Eng Med Biol 12: 26–39.

Van Essen DC, Drury HA. (1997): Structural and functional analyses of human cerebral cortex using a surface-based atlas. J Neurosci 17:7079–7102.

Van Essen DC, Lewis JW, Drury HA, Hadjikhani N, Tootell RB, Bakircioglu M, et al. (2001): Mapping visual cortex in monkeys and humans using surface-based atlases. Vision Res 41:1359–1378.

Vesalius A. (1543): De humani corporis fabrica libri septem. Basilea: Ex officina I. Oporini.

Watkins KE, Paus T, Lerch JP, Zijdenbos A, Collins DL, Neelin P, et al. (2001): Structural asymmetries in the human brain: a voxel-based statistical analysis of 142 MRI scans. Cereb Cortex 11:868–877.

Westbury CF, Zatorre RJ, Evans AC. (1999): Quantifying variability in the planum temporale: a probability map. Cereb Cortex 9:392–405.

Woods RP, Mazziotta JC, Cherry SR. (1993): MRI-PET registration with automated algorithm. J Comp Assist Tomogr 17:536–546.

Yousry TA, Schmid UD, Alkadhi H, Schmidt D, Peraud A, Buettner A, et al. (1997): Localization of the motor hand area to a knob on the precentral gyrus. A new landmark. Brain 120:141–157.

Zilles K, Schleicher A, Langemann C, Amunts K, Morosan P, Palomero-Gallagher N, et al. (1997): Quantitative analysis of sulci in the human cerebral cortex: development, regional heterogeneity, gender difference, asymmetry, inter-subject variability and cortical architecture. Hum Brain Mapp 5:218–221.

APPENDIX: DELINEATION ALGORITHM

The algorithm was developed from a previously defined protocol for the segregation of neuroanatomical structures. Each volume is described in terms of its defining boundaries in each dimension. When this is insufficient, footnotes are used.

Structures 1 and 2: Hippocampus (right; left)[1]

Orientation of slices	Coronal
Anterior border	First slice = most anterior slice where temporal horn loses it slit like appearance, widens and lies next to hippocampus. Include subiculum in measurement anteriorly.
Posterior border	Last slice = slice anterior to that where cella media, temporal horn, and occipital horn fuse. Exclude the fornix on last slice as cannot be separated from the crura fornicis
Medial border	Parahippocampal gyrus: CSF
Lateral border	Anterior → posterior: Lateral ventricle; WM
Superior border	Anterior → posterior: Amygdala; lateral ventricle
Inferior border	Parahippocampal gyrus; uncal sulcus; interface of the prosubiculum and cornu ammonis; border between subiculum, and praesubiculum; sulcus hippocampalis
Number of slices	~25

Structures 3 and 4: Amygdala (right; left)

Orientation of slices	Coronal
Anterior border	End of clear distinction between nucleus corticalis and adjacent cortex
Posterior border	End of amygdala (at this level dorsolaterally to digitatio verticalis hippocampi, in dorsal ventricular wall)
Medial border	Anterior → posterior: Cisterna chiasmatis and ambiens; previously outlined parts of hippocampus
Lateral border	WM
Superior border	Sulcus endorhinalis
Inferior border	Anterior → posterior: WM; ventricle/hippocampus
Number of slices	~15

[1] See Niemann K, et al. [2000a]. In the coronal orientation, the hippocampus has four distinct shapes when progressing posteriorly. The first is "boomerang-like." Three rules were applied to differentiate the hippocampal head from the amygdala in these anterior slices exhibiting shape one: (1) The dorso-medial corner of the temporal horn of the lateral ventricle indicated the position of the frontal cleft at the interface of the amygdala and hippocampus; (2) the myelin layer of the alveus of the hippocampus was used as a differentiator; and (3) when rules 1 and 2 were insufficient, a region of low signal could frequently be seen defining the border. This has been attributed to either partial volume effect due to a narrow cleft, or small vessels between the two structures. Shape two has been likened to a rabbit with its "head" medially, and the digitatio verticalis as its "ears." When this shape was evident, the uncal sulcus was used as the inferior border. At the lateral end of this sulcus, a line was drawn at 45 degrees to the horizontal in a basolateral direction to approximate the interface of the prosubiculum and cornu ammonis. The third shape of the hippocampus has been compared with binoculars. If the uncal sulcus was no longer visible this far posteriorly, the border between the hypointense subiculum, and the hyperintense praesubiculum was used as the inferior border. The fourth shape is the first through the hippocampal body; at this point both the subiculum and fimbria were included in the measurement, and the hippocampal, not uncal, sulcus was used as the inferior border.

APPENDIX: (continued)

Structures 5 and 6: Anterior temporal lobe, medial part (right; left)[2]

Orientation of slices	Coronal
Anterior border	Temporal pole
Posterior border	First slice = slice anterior to the anterior end of amygdala
Medial border	CSF (cisterna valleculae cerebri → cisterna ambiens)
Lateral border	Lateral part of anterior temporal lobe
Superior border	CSF; posteriorly, eventually temporal stem (then draw a straight line between most superior lateral & medial border)
Inferior border	CSF
Number of slices	~25

Structures 7 and 8: Anterior temporal lobe, lateral part (right; left)[2]

Orientation of slices	Coronal
Anterior border	Temporal pole
Posterior border	First slice = slice anterior to the anterior end of amygdala
Medial border	Medial part of anterior temporal lobe
Lateral border	CSF
Superior border	CSF; posteriorly, eventually temporal stem (then draw a straight line between most superior lateral & medial border)
Inferior border	CSF
Number of slices	~25

Structures 9 and 10: Parahippocampal and ambient gyri (right; left)[3]

Orientation of slices	Coronal
Anterior border	Anterior end of amygdala as previously defined (that slice included)
Posterior border	Posterior border of hippocampus as previously defined (that slice included)
Medial border	Cisterna ambiens
Lateral border	Anterior → posterior: Sulcus collateralis (not sulcus rhinalis) and superiorly towards amygdala previously defined/most lateral extent of temporal horn of lateral ventricle, subdividing the WM like the spokes of a wheel
Superior border	Hippocampus and amygdala as previously defined
Inferior border	Cisterna ambiens/sulcus collateralis
Number of slices	~25

[2] The border dividing the medial and lateral portions of the anterior temporal lobe was defined in the original protocol as the sulcus temporalis inferior. The nature of this sulcus was highly variable; it was not present throughout the anterior portion of every temporal lobe analysed. Therefore, it was not possible to rely on this sulcus as a consistent feature for division of the two portions. This observation is supported by Ono et al. [1990], who reported that the sulcus separates in 16 and 52% of anterior temporal lobes on the right and left, respectively, and is absent at the tip of 4% of temporal lobes. The division of the two portions of the anterior lobe was redefined using a radial divider tool within the software (Analyze). This divides a described region into a predetermined number of segments (in this case two) as radiations from a point defined by the centre of the area of the region. Thus, it was possible to provide a consistent definition of the two portions of the temporal lobe.

[3] The course of the sulcus collateralis can be very variable, and may frequently be interrupted and/or duplicated as one progresses from its anterior to posterior extent. Consequently, in many of the datasets the path of this sulcus became impossible to determine for a few slices. In such cases, the protocol was refined to include the use of the transverse orientation to extrapolate a projected course over the slices in question.

APPENDIX: (continued)

Structures 11 and 12: Superior temporal gyrus (right; left)[4]

Orientation of slices	Coronal
Anterior border	First slice = most anterior slice where amygdala is measured
Posterior border	Last slice = most posterior slice where hippocampus is measured
Medial border	Draw a line radially to the lateral inferior horn of the lateral ventricle or, if the ventricle is not discernable, to the most lateral extent of the hippocampus (amygdala anteriorly). Line comes from most inferior end of sulcus circularis insulae and most medial end of sulcus temporalis superior, respectively. These lines end in a short line rather than a point to include some of the WM (see examples)
Lateral border	CSF
Superior border	Sulcus lateralis, thus including the planum temporale in the structure's posterior portion
Inferior border	Sulcus temporalis superior
Number of slices	~25

Structures 13 and 14: Middle and inferior temporal gyri (right; left)

Orientation of slices	Coronal
Anterior border	First slice = most anterior slice where amygdala is measured
Posterior border	Last slice = most posterior slice where hippocampus is measured
Medial border	Sulcus occipitotemporalis; from superior end draw a line radially to the most lateral extent of the inferior horn of the lateral ventricle or, if the ventricle is not discernable, to the most lateral extent of the hippocampus (amygdala anteriorly).
Lateral border	CSF
Superior border	Sulcus temporalis superior; from medial end draw a line radially to the most lateral extent of the inferior horn of the lateral ventricle or, if the ventricle is not discernable, to the most lateral extent of the hippocampus (amygdala anteriorly).
Inferior border	CSF
Number of slices	~25

Structures 15 and 16: Lateral occipitotemporal gyrus (fusiform gyrus) (right; left)

Orientation of slices	Coronal
Anterior border	First slice = most anterior slice where amygdala is measured
Posterior border	Last slice = most posterior slice where hippocampus is measured
Medial border	Sulcus occipitotemporalis
Lateral border	Sulcus collateralis
Superior border	From the superior ends of sulcus occipitotemporalis and sulcus collateralis draw a line radially to the most lateral extent of the inferior horn of the lateral ventricle or, if the ventricle is not discernable, to the most lateral extent of the hippocampus (amygdala anteriorly).
Inferior border	CSF
Number of slices	~25

[4] The use of the sagittal orientation facilitated more accurate determination of the sulci that bound the superior temporal gyrus. Similarly, the transverse orientation was used with the middle and inferior temporal gyri.

APPENDIX: (continued)

Structures 17 and 18: Cerebellum (right; left)[5]

Orientation of slices	Sagittal
Anterior border	Cut cerebellar peduncle parallel to floor of IVth ventricle beginning on the slice where the cerebellar peduncle joins the brainstem (pons)
Posterior border	CSF
Medial border	Midline
Lateral border	CSF/sinus transversus (lateral sinus)
Superior border	CSF/tentorium cerebelli
Inferior border	CSF
Number of slices	~55

Structure 19: Brainstem (spans the midline)

Orientation of slices	Sagittal
Anterior border	CSF
Posterior border	CSF/cut from cerebellum as described under "Cerebellum"
Medial border	No medial border; spans the midline
Lateral border	CSF, pons/midbrain: as soon as the cerebellar peduncle is no longer in contact with the pons, the posterior remainder is measured together with the cerebellum; the superior remainder is measured with the basal ganglia
Superior border	Cut from basal ganglia as soon as pedunculus cerebri enters them using a tangential line following the contours of the basal ganglia
Inferior border	Inferior border of cerebellum
Number of slices	~30

Structures 20 and 21: Insula (left; right)

Orientation of slices	Coronal
Anterior border	Last slice on which sulcus circularis insulae is visualized
Posterior border	Last slice on which sulcus circularis insulae is visualized
Medial border	Lateral border of putamen (draw a line from medial end of sulcus circularis insulae); if no longer visible, use anterior lateral border of caput nuclei caudati or lateral border of lateral ventricle, respectively; posteriorly use lateral border of thalamus instead
Lateral border	CSF in sulcus lateralis
Superior border	Sulcus circularis insulae
Inferior border	Sulcus circularis insulae
Number of slices	~70

Caution: left, then right; start by estimating anterior–posterior extent with sagittal slices.

[5] The anterior border thus defined corresponds to the Spielmeyer cut.

APPENDIX: (continued)

Structures 22 and 23: Occipital lobe (left; right)

Orientation of slices	First sagittal, then transverse
Sagittal cuts (start medially)	
Anterior border	Sulcus parieto-occipitalis
Posterior border	CSF
Medial border	Midline
Lateral border	Last slice on which sulcus parieto-occipitalis is visible in its full length (then change to transverse cuts)
Superior border	Sulcus parieto-occipitalis and CSF
Inferior border	Tentorium cerebelli/CSF
Transverse cuts	
Anterior border	Straight line between medial end of sulcus occipitalis anterior, and lateral end of sulcus parieto-occipitalis
Posterior border	CSF
Medial border	As previously defined on sagittal cuts
Lateral border	CSF
Superior border	Parietal lobe (sulcus occipitalis anterior)
Inferior border	CSF/tentorium cerebelli
Number of slices	~85

Structures 24 and 25: Gyrus cinguli, anterior part (left; right)

Orientation of slices	Transverse, then sagittal, then return to transverse
Inferior border	Define on the most inferior slice on which genu corporis callosi is uninterrupted throughout its width (see Figure 3).
Sagittal cuts	
Anterior border	Sulcus cinguli
Posterior border	Draw vertical line from corpus callosum to sulcus cinguli at the mid-point of the greatest extension of the corpus callosum (measured using coordinates of region of interest module of Analyze AVW) on most medial slice; corpus callosum inferiorly
Medial border	Midline
Lateral border	Last slice on which sulcus cinguli is visible in its full length (then change to transverse cuts)
Superior border	Sulcus cinguli; if double sulcus cinguli present (Ono et al., 1991) choose dorsal/anterior one.
Inferior border	As defined in transverse orientation
Transverse Cuts	
Lateral border	Re-defined as straight line posteriorly from anterior-lateral end of sulcus cinguli on superior slices.
Anterior border; posterior border; medial border; superior border; inferior border	As previously defined on sagittal cuts
Number of slices	~50

APPENDIX: (continued)

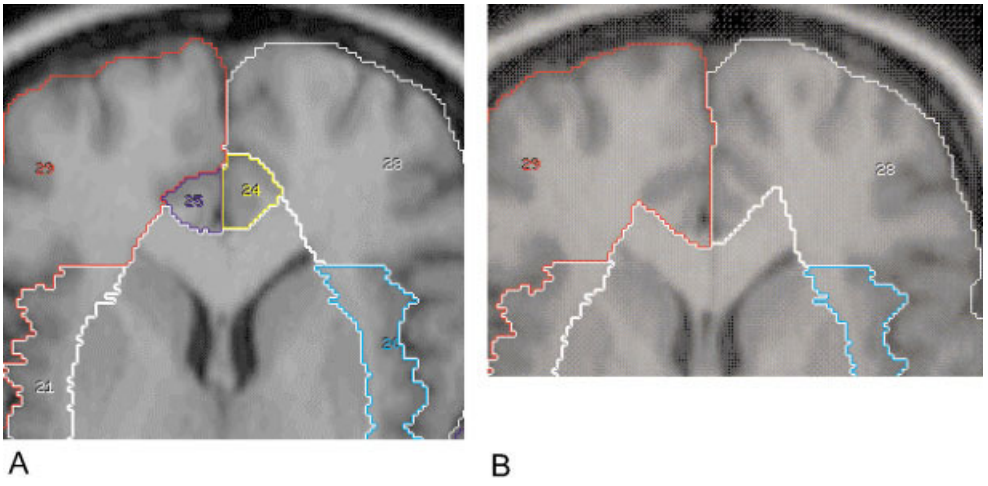

Figure 3.
The genus of the corpus callosum: a continuous throughout its entire width; b interrupted (see structures 24 and 25).

Structures 26 and 27: Gyrus cinguli, posterior part (left; right)

Orientation of slices	Transverse, then sagittal, then return to transverse
Inferior border	Define on the most inferior slice on which splenium corporis callosi is uninterrupted throughout its width (see Figure 4).
Sagittal cuts	
Anterior border	Gyrus cinguli, anterior part
Posterior border	Sulcus subparietalis; inferiorly, sulcus parieto-occipitalis
Medial border	Midline
Lateral border	Last slice on which sulcus cinguli is visible in its full length (then change to transverse cuts)
Superior border	sulcus cinguli; if double sulcus cinguli present (Ono et al., 1991) choose dorsal/posterior one.
Inferior border	As defined in transverse orientation
Transverse cuts	
Lateral border	Re-defined as straight line anteriorly from posterior-lateral end of sulcus cinguli on superior slices.
Anterior border; posterior border; medial border; superior border; Inferior border	As previously defined on sagittal cuts
Number of slices	~50

APPENDIX: (continued)

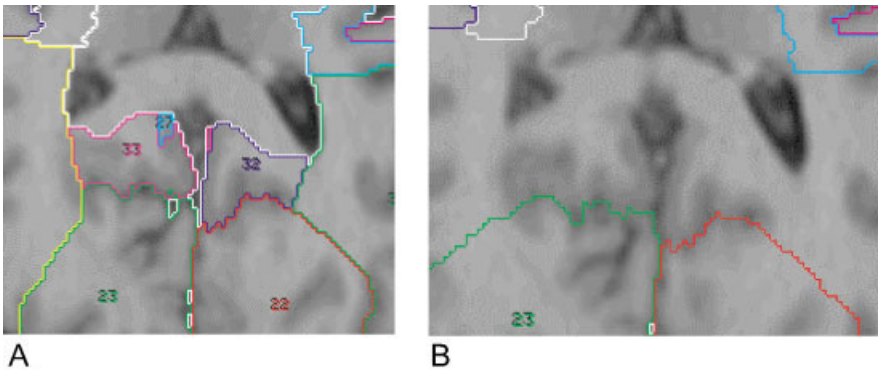

Figure 4.
The splenium of the corpus callosum: a continuous throughout its entire width; b interrupted (see structures 26 and 27 and footnote 6).

Structures 28 and 29: Frontal lobe (left; right)

Orientation of slices	Transverse
Anterior border	CSF
Posterior border	Superior → inferior: Sulcus centralis → line orthogonal to midline from medial end of sulcus centralis to interhemispheric fissure/gyrus cinguli/corpus callosum/lateral ventricle/striatum/insula → CSF in most inferior portion.
Medial border	Superior → inferior: Interhemispheric fissure → gyri cinguli → corpus callosum → lateral border of lateral ventricle → lateral border of striatum/insula → interhemispheric fissure
Lateral border	CSF
Superior border	CSF
Inferior border	CSF
Number of slices	~105

Caution: Start superiorly to reliably identify central sulcus

Structures 30 and 31: Posterior temporal lobe (left; right)[6]

Orientation of slices	Transverse
Anterior border	Straight horizontal line marking the last coronal cut of the temporal lobe (see structures 8–11); include temporal operculum up to superior border
Posterior border	Cerebellum and occipital lobe as previously defined
Medial border	Cerebellum and occipital lobe; cisterna ambiens; cisterna venae cerebri magnae; splenium of corpus callosum; lateral ventricle; midline
Lateral border	CSF
Superior border	Last slice on which the posterior border(s) of any of structures 9–16 occupied the majority (greater than 50%) of the space between CSF laterally, and non-temporal lobe structures medially.
Inferior border	CSF
Number of slices	~45

[6] In the more inferior slices where the splenium was absent or non-continuous, the lateral ventricle was included in the definition of the posterior temporal lobe on the medial side. However, in the slices where the splenium was continuous (see Fig. B), the lateral ventricle and splenium were excluded.

APPENDIX: (continued)

Structures 32 and 33: Parietal lobe (left; right)[7]

Orientation of slices	Transverse
Anterior border	Previously defined structures
Posterior border	Previously defined structures; CSF
Medial border	Midline; previously defined structures; corpus callosum; ventricle; basal ganglia
Lateral border	CSF
Superior border	CSF
Inferior border	Previously defined structures
Number of slices	~60

Caution: The parietal operculum, and praecuneus are included in the definition of the parietal lobe.

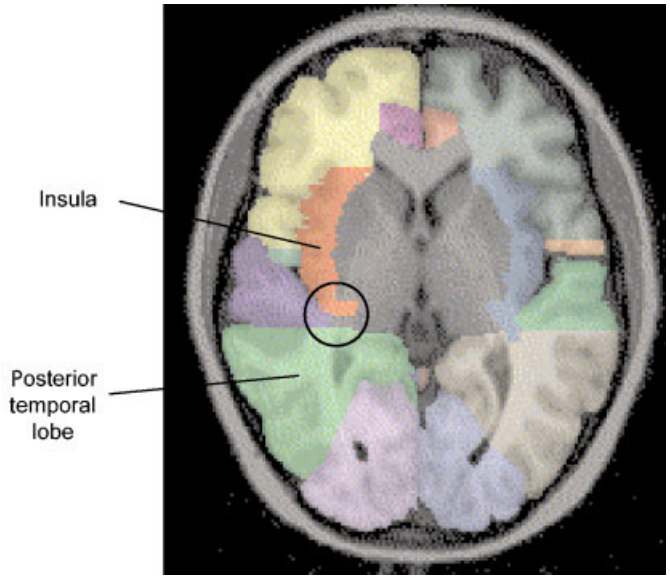

Figure 5.
In some datasets, the insula did not extend as far posteriorly as the structures of the mid-part of the temporal lobe (circled). (See structures 32 and 33 and footnote 7).

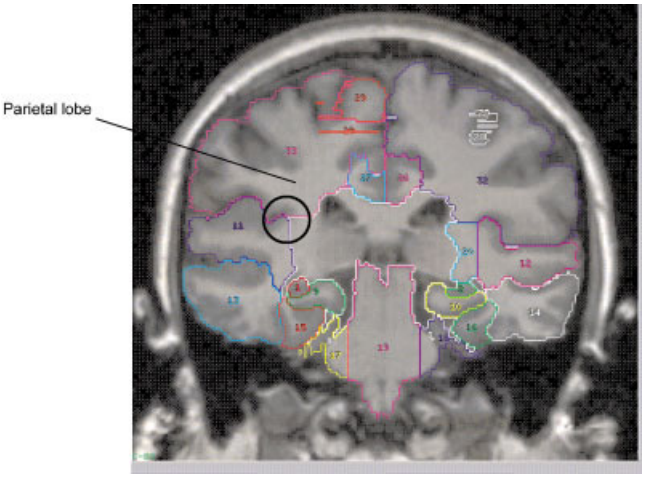

Figure 6.
Validation of the inferior border of the parietal lobe (circled; see structures 32 and 33 and footnote 7).

[7] The border with the corpus callosum was defined through a line between the occipital horn of the lateral ventricle and the gyrus cinguli. This line crosses the corpus callosum as it becomes confluent with the WM of the parietal lobe. The posterior border of the insula was defined as the last slice containing sulcus circularis insulae. Sometimes the insula did not extend as far posteriorly as the structures of the mid-part of the temporal lobe (structures 9–16; see Figure 5). In these circumstances, an undefined WM region exists. Superiorly, this area is bounded by, and was included in, the parietal lobe. However, more inferiorly, the region in question was only included in the definition of the parietal lobe when it was continuous with other areas labeled parietal lobe. The coronal orientation was used to ensure the validity of this rule, and revealed that the cut-off point represented the border with the most superior aspects of the temporal lobe (see Figure 6).

APPENDIX: (continued)

Structures 34 and 35: Caudate nucleus (left, right)

Orientation of slices	Transverse
Anterior border	Superior to inferior: frontal lobe and/or corpus callosum, then lateral ventricle, corpus callosum, frontal lobe
Posterior border	Superior to inferior: lateral ventricle, internal capsule/anterior commissure
Medial border	Superior to inferior: lateral ventricle/corpus callosum, frontal lobe as previously defined, following the intensity gradient of the caudate avoiding the medial gray matter adjacent to the CSF
Lateral border	Superior to inferior: frontal/parietal lobe as previously defined, internal capsule, internal capsule/insula
Superior border	Start on first slice where on which caudate is visible at the lateral border of the lateral ventricle
Inferior border	Retaining the medial border, continue defining the caudate until frontal lobe as defined previously is reached. This border is subsequently edited in coronal orientation when defining the accumbens as a substructure of the caudate region as outlined here (see structures 36 and 37).
Number of slices	~30

Caution: This protocol includes the Nucleus accumbens which subsequently will be redefined as a separate structure.

Structures 36 and 37: Nucleus accumbens (left, right)

Orientation of slices	Coronal; start posteriorly.
Anterior border	Last slice where accumbens can be clearly differentiated from the caudate.
Posterior border	First slice where the inferior part of the previously defined caudate region is seen (e.g., inferior of the anterior commissure), separated from the superior bulk of the caudate region. This separated section represents the accumbens.
Medial border	Do not change.
Lateral border	Do not change.
Superior border	Nucleus accumbens is always inferior to the lateral ventricle. Anterior to where the separated parts of the previously defined caudate region merge, the superior border is defined through its shape and a slightly more hypointense appearance than the caudate itself.
Inferior border	Smooth previously defined border and exclude white matter and the medial gray matter adjacent to the CSF, impinge on previously defined frontal lobe region if necessary.
Number of slices	~8

Caution: This protocol requires the prior definition of accumbens and caudate together on transverse slices as outlined above (see structures 34 and 35). The new regions need to be renumbered.

Structures 38 and 39: Putamen (left, right)

Orientation of slices	Transverse
Anterior border	Frontal lobe, internal capsule, insula in varying combinations as previously defined
Posterior border	Internal capsule
Medial border	Superior to inferior: Internal capsule, lamina medullaris lateralis, substantia perforata anterior
Lateral border	Superior to inferior: frontal lobe/parietal lobe, insula
Superior border	Most superior slice where putamen is seen
Inferior border	Frontal lobe. The coronal orientation can be useful to verify the borders.
Number of slices	~25

APPENDIX: (continued)

Structures 40 and 41: Thalamus (left, right)

Orientation of slices	Coronal
Anterior border	End of anterior thalamic nucleus at foramen Monroi
Posterior border	First slice where pulvinar is visible
Medial border	Posterior to anterior: Cisterna ambiens/laminae tecti, corpus callosum, third ventricle/midline at adhaesio interthalamica
Lateral border	Posterior to anterior: posterior temporal lobe white matter, insula as previously defined, internal capsule
Superior border	Posterior to anterior: white matter/corpus callosum, lateral ventricle, stria terminalis/vena thalamostriata
Inferior border	Posterior to anterior: cisterna ambiens, temporal lobe as previously defined (include both medial and lateral geniculate body, adjust temporal lobe regions where necessary)
Number of slices	~30

Caution: Start posteriorly

Structures 42 and 43: Pallidum (left, right)

Orientation of slices	Coronal
Anterior border	First slice where visible (pars lateralis, within internal capsule)
Posterior border	Last slice where visible
Medial border	Internal capsule
Lateral border	Lamina medullaris lateralis/putamen
Superior border	Internal capsule
Inferior border	Anterior to posterior: White matter of subcallosal gyrus, anterior commissure, white matter superior to anterior perforated substance/amygdala/hippocampus
Number of slices	~20

Caution: Do not include lamina medullaris lateralis

Structure 44: Corpus callosum

Orientation of slices	Transverse
Anterior border, anterior part	Superior to inferior: cingulate gyrus and frontal lobe → frontal lobe
Anterior border, posterior part	Superior to inferior: lateral ventricle, fornix, cisterna fissurae transversae cerebri → idem thalamus
Posterior border, anterior part	Superior to inferior: lateral ventricle → caudate/nucleus accumbens
Posterior border, posterior part	Superior to inferior: posterior cingulate gyrus and parietal lobe → idem and interhemispheric CSF
Medial border	Superior to inferior: cingulate gyri as soon as the corpus callosum appears X-shaped → frontal/parietal lobe → idem and posterior temporal lobes → head of caudate anteriorly
Lateral border	Superior to inferior: frontal and parietal lobes → idem and lateral ventricle
Superior border	Defined through remainder after delineation of cingulate gyri and frontal and parietal lobes.
Inferior border	Anteriorly, last slice on which the corpus callosum can be clearly distinguished; posteriorly, inferior end of splenium
Number of slices	~35

Caution: Do not include fornix.

APPENDIX: (continued)

Structures 45 and 46: Lateral ventricle, frontal horn, central part and occipital horn (right, left)

Orientation of slices	Transverse
Anterior border, anterior part	CC
Anterior border, posterior part	Superior to inferior: thalamus → unnamed region behind thalamus/posterior of insula → posterior temporal lobe → anterior border of posterior temporal lobe region (see structures 47 and 48)
Posterior border, anterior part	Superior to inferior: thalamus → thalamus/fornix/capsula interna, caput nuclei caudati
Posterior border, posterior part	Superior to inferior: parietal lobe → corpus callosum → parietal lobe/posterior temporal lobe/occipital lobe
Medial border, anterior part	Superior to inferior: corpus callosum → septum pellucidum/fornix → basal forebrain.
Medial border, posterior part	Superior to inferior: corpus callosum → medial parietal lobe/posterior temporal lobe
Lateral border, anterior part	Superior to inferior: frontal and parietal lobes → plus corpus nuclei caudati → caput nuclei caudati → plus frontal lobe
Lateral border, posterior part	Superior to inferior: frontal and parietal lobes → plus corpus nuclei caudati → posterior temporal lobe
Superior border	First slice where ventricle visible, include part with partial volume effect
Inferior border, anterior part	End of CSF in frontal lobe
Inferior border, posterior part	End of CSF in posterior temporal lobe that lies posterior to the anterior border of the posterior temporal lobe region
Number of slices	~35

Caution: right, then left. Use CSF partition of segmented MRI as related volume to aid in delineation, use autotrace function for posterior part inferiorly after CC disappears.

Structures 47 and 48: Lateral ventricle, temporal horn (right, left)

Orientation of slices	Coronal
Anterior border	First appearance of CSF
Posterior border	Last slice on which hippocampus is still delineated = last slice anterior to posterior temporal regions (see structure 45 and 46)
Medial border	Anterior to posterior: parahippocampal gyrus/hippocampus/amygdala → hippocampus/choroid fissure → fimbria/crus fornicis
Lateral border	Anterior to posterior: parahippocampal gyrus or temporal lobe white matter
Superior border	Anterior to posterior: amygdala → temporal white matter (temporal stem)
Inferior border	Anterior to posterior: temporal lobe white matter → plus hippocampus
Number of slices	~25

Caution: may only be intermittently visible. Use CSF partition of segmented MRI as related volume to aid in delineation.

Structure 49: Third ventricle

Orientation of slices	Coronal
Anterior border	Lamina terminalis
Posterior border	Pineal gland, include recessus pinealis/suprapinealis
Medial border	None (single structure)
Lateral border	Anterior to posterior: hypothalamus → thalamus → nuclei habenularum
Superior border	Anterior to posterior: lamina terminalis → anterior commissure/columna fornicis → foramen Monroi → tela choroidea (caution does not exceed height of adhaesio interthalamica posterior to it; do not confound internal cerebral veins superior of tela choroidea)
Inferior border	Anterior to posterior: chiasma opticum → infundibulum → hypothalamus → posterior commissure
Number of slices	~35

Caution: Use sagittal for help with posterior extent first. Use CSF partition of segmented MRI as related volume to aid in delineation.